Investigation of Microstructure of Laser Cladding Ni-WC Layer on Al-Si Alloy

G.Y. Liang and T.T. Wong

A plasma-sprayed Ni-WC layer was deposited on an Al-Si cast alloy surface, and then it was further melted by a 5 kW CO_2 laser. The microstructure and chemical composition of the laser-melted zone were investigated, and the microhardness in different parts was measured.

Experimental results showed that the chemical composition of the sample was not uniform. Compositional segregation in the laser-melted zone was found. Some amorphous structure appeared in the nickel-rich locations after laser melting. Owing to the thermal effect of the laser scanning, an intermediate-phase Ni_3Al segregated from this region and formed Ni_3Al grains and amorphous grains. Some WC particles melted in the matrix, and chromium carbide $Cr_{23}C_6$ and (Cr,W)C separated during the cooling process. The highest microhardness (1027HV) was found in the high-nickel region.

Keywords
aluminum, amorphous structure, laser surface cladding, microstructure

1. Introduction

LASER CLADDING has been developed as a method for producing coatings to enhance the surface resistance of materials against wear, corrosion, and high-temperature oxidation (Ref 1-3).

Aluminum alloys are widely used in many technological fields because of their low density, high thermal conductivity, and good corrosion resistance in atmosphere. However, their hardness is fairly low and their friction and abrasive properties are very poor. In order to improve their wear resistance, it is necessary to increase their surface hardness and to change their surface structure. Recent studies (Ref 4-6) show that laser melting and cladding of aluminum alloys can effectively improve their surface properties and wear resistance.

Ni-WC powder is a commercial alloy material that is often used in the plasma and thermal spraying of iron and steel surfaces. It has high hardness and good strength and corrosion resistance. Because this powder contains WC ceramic and possesses a high melting point, it is difficult to deposit it on aluminum alloys. Using plasma spraying and laser surface melting, it is possible to deposit a high-melting material onto a low-melting material to form a surface layer with good wear resistance and heat resistance. In this paper, a plasma-sprayed coating was surface melted by laser on an Al-Si alloy surface, and the microstructure and existence of WC were investigated.

2. Experimental Procedure

The substrate sample was an Al-Si cast alloy. Its chemical composition is shown in Table 1. It was machined into rectangular plates 50 by 35 by 10 mm. After hot NaOH etching and sandblasting, the sample surface was sprayed by Type METCO 4HC Plasma Spray Unit. The sprayed powder was commercial Ni-WC alloy, which has the chemical composition shown in Table 2. The thickness of the sprayed coating was about 0.4 mm.

The surface melting operation was subsequently conducted with a 5 kW continuous transverse flow CO_2 laser. During the operation, the laser beam was focused to a diameter of 2.5 mm, the incident power density of the laser beam was 65.2 kW/cm^2, and the transverse laser velocity along the surface was 10 mm/s. The sample surface was protected by argon gas during the laser scanning. The total depth of laser melted zone was 1.5

Table 1 Chemical composition of base metal

Elements	Si	Mg	Cu	Ti	Mn	Al
wt%	8.23	0.056	1.35	0.057	0.5	bal

Table 2 Chemical composition of thermal spraying alloy powder

Elements	Cr	B	Si	Fe	C	WC	Ni
wt%	10.5	1 2	1.5	10	<1.0	20	bal

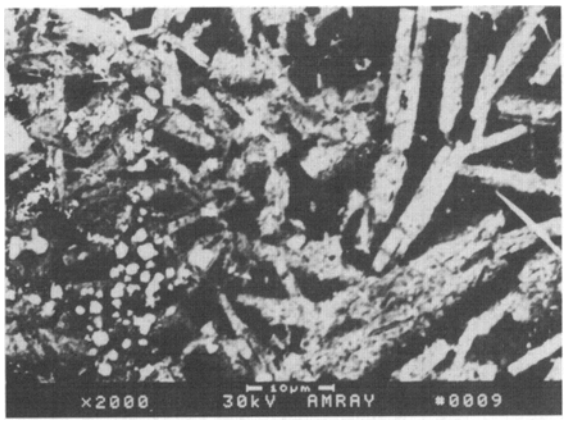

Fig. 1 SEM photo of the surface of the laser-melted zone

G.Y. Liang, Xian Jiaotong University, Xian, China; and **T.T. Wong,** The Hong Kong Polytechnic University, Hong Kong.

mm, which consisted of the laser-alloyed zone and melted aluminum substrate. The thickness of the laser-alloyed zone was about 0.5 mm.

A cross section of the sample perpendicular to the direction of laser scanning was prepared. A thin foil about 0.5 mm thick was cut from the top of the laser-melted zone of the sample. Af-

Table 3 Chemical composition of phases shown in Fig. 1 to 3

Elements		Al	Cr	Fe	Si	W	Ni
Needle-like phase in Fig. 1	at.%	47.95	1.08	9.33	6.70	2.16	32.78
	wt%	29.48	1.27	11.90	4.27	9.03	44.07
$Cr_{23}C_6$ phase in Fig. 2 (part A)	at.%	10.90	58.25	10.11	2.72	2.10	15.91
	wt%	5.56	57.24	10.70	1.44	7.31	17.74
(Cr,W)C phase in Fig. 2 (part B)	at.%	9.42	53.71	2.87	0.10	14.56	7.86
	wt%	3.89	42.68	2.46	0.04	40.90	7.05
WC phase in Fig. 3	at %	6 59	0.03	3.75	31.04	54.86	3.73
	wt%	1.54	0.01	1.81	7.51	87.23	1.90

Table 4 Chemical composition of each structure in Fig. 4

Elements		Al	Cr	Fe	Si	W	B	Ni
Average compositiona	at.%	28.32	4.25	6.15	5 93	3.60	3.64	48.11
	wt%	15.18	4.38	6.83	3.30	13.15	0.78	56.36
Precipitate	at.%	24.09	1.55	3.48	4.12	3.57	4.16	59.03
	wt%	12.44	1.63	3.72	2.21	12.55	0.86	66.58
Spaces between precipitates	at.%	33.33	11.40	8.87	10.14	3.62	2.42	30.09
	wt%	18.82	13.11	10.39	5.94	13.93	0.55	37.35

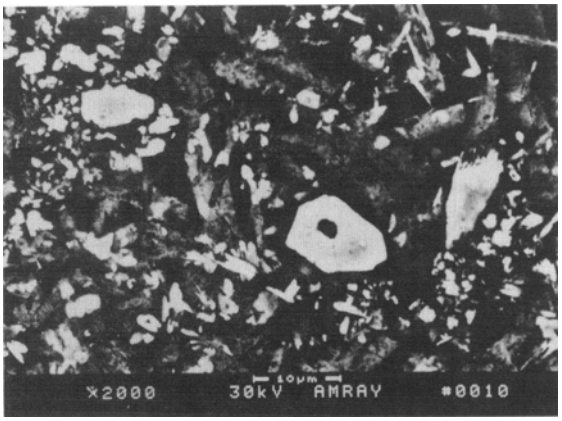

Fig. 2 SEM photo of the interior of the laser-alloyed zone

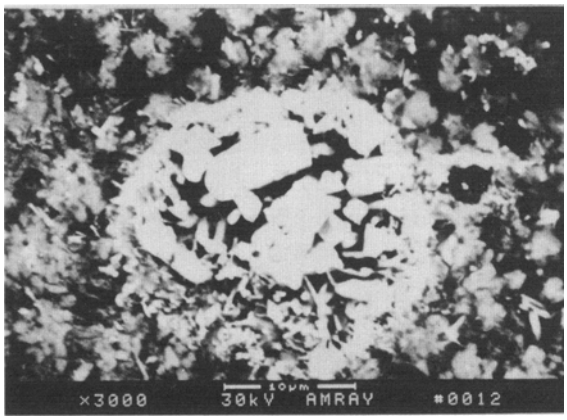

Fig. 3 SEM photo of the interior of the laser-alloyed zone

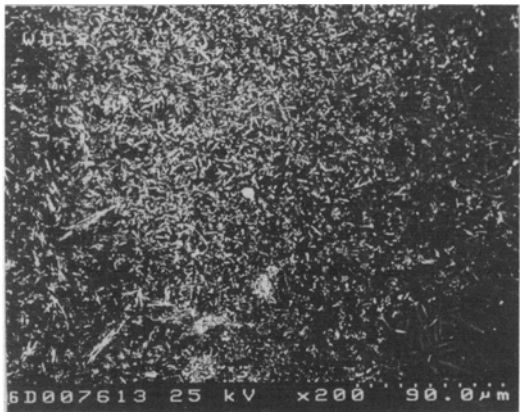

(a)

(b)

Fig. 4 SEM photos of the subsurface of the laser-melted zone. (a) Low magnification, 200×. (b) High magnification, 2000×

ter the thickness was reduced to 0.1 mm, a film specimen for transmission electron microscopy was made by ion thinning. The examination of the microstructure employed a type S-2700 scanning electron microscope (SEM) and a type JEM-200CX transmission electron microscope (TEM). Microhardness was measured using a type HX-1000 Vickers Hardness Meter. The loading was 50 g and the loading time was 15 s during the hardness test.

3. Experimental Results and Discussion

3.1 *Microstructure and Microprobe Analysis*

Figure 1 is a SEM photo of the surface of the laser-melted zone of the sample. There are a lot of needlelike phases and a few precipitated phases in this region. Figure 2 is a SEM photo of the interior of the laser-alloyed zone. Precipitated phases can be seen. The morphology of these phases suggests that they are composed of $Cr_{23}C_6$ and (Cr,W)C. In another SEM photo in this region (Fig. 3), a cluster of unmelted WC particles is surrounded by the matrix. The chemical composition of the phases in Fig. 1 to 3 is shown in Table 3.

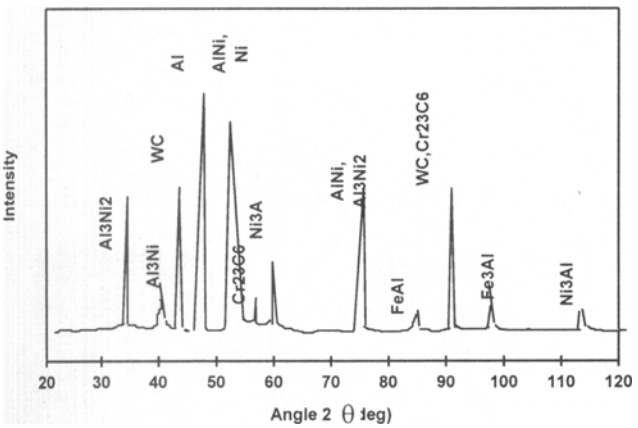

Fig. 5 X-ray diffraction diagram of the laser-alloyed zone

According to Table 3 and the Al-Ni binary alloy phase diagram (Ref 7), we can infer that the needlelike phase in Fig. 1 is type Al_3Ni_2-based intermetallic compound, which also contains Fe, Cr, and W. In Fig. 2, phases $Cr_{23}C_6$ and (Cr,W)C are present because the initial WC deposit was melted and nucleated again. Because the melting point of WC is very high, some WC particles are unmelted in the laser melt so that they are surrounded by the laser-alloyed zone.

Beneath the surface of the laser-melted zone, there exist some roll-like structures. Figure 4(a) is a low-magnification SEM photo of the subsurface. It is located under the needlelike structure zone shown in Fig. 1. Figure 4(b) is a high-magnification photo of the subsurface. We can see some granular and small rodlike precipitates. Beneath these precipitates, there exist some glasslike structures (arrow). The chemical composition of the different structures shown in Fig. 4 is given in Table 4.

From Table 4, we can see that the average composition of the fine granular region is higher in nickel than that of the surface. The composition of the precipitate is similar to that of phase Ni_3Al, and the composition of the spaces between the precipitates is about the same as that of the spaces between the NiAl particles.

3.2 *Structure Analysis*

Figure 5 is an X-ray diffraction diagram of the laser-alloyed zone on the aluminum alloy. In this figure, it is seen that there

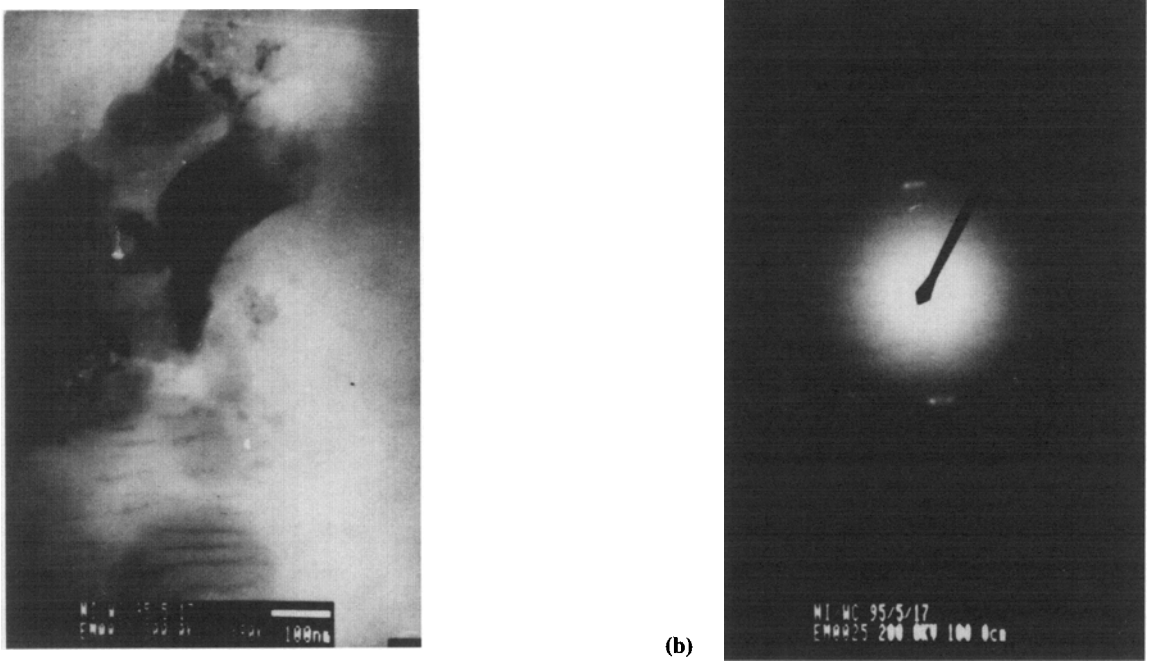

Fig. 6 TEM photo of the laser-alloyed zone. (a) Bright field. (b) Diffraction pattern

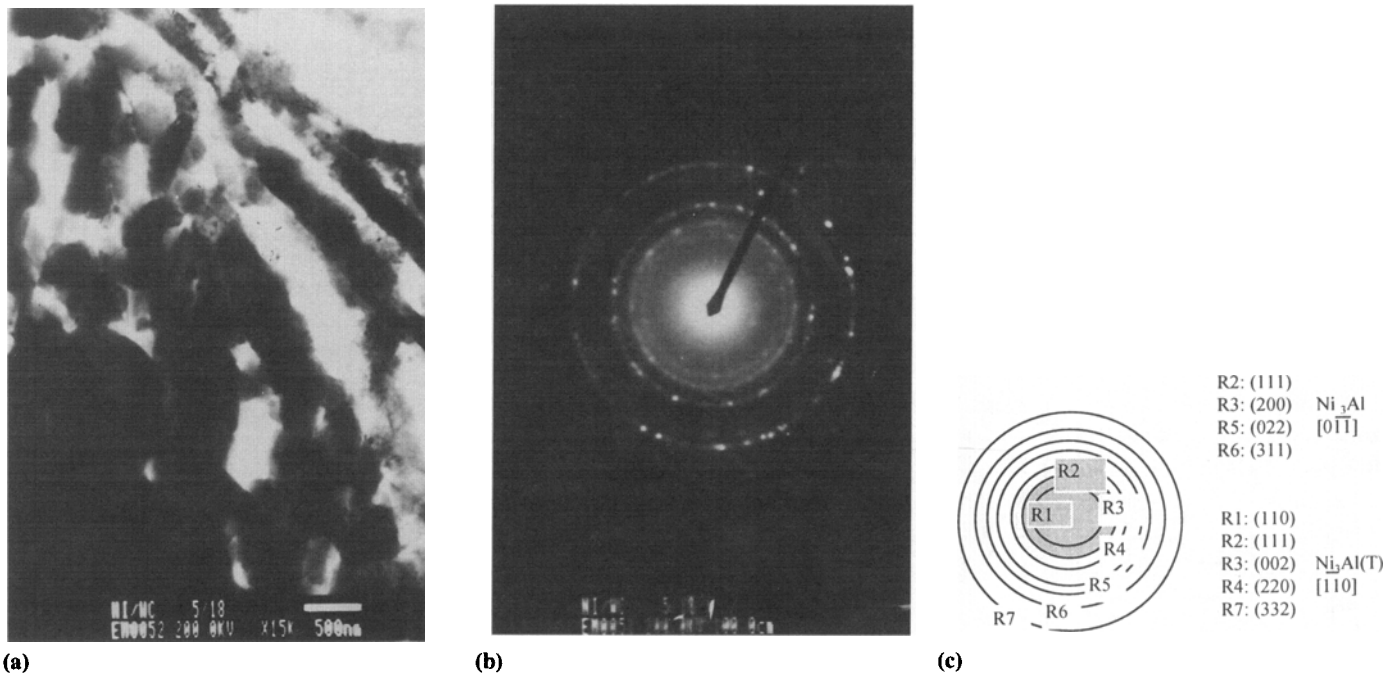

Fig. 7 TEM photo of the fine granular region of the laser-alloyed zone. (a) Bright field. (b) Diffraction pattern. (c) Indexing

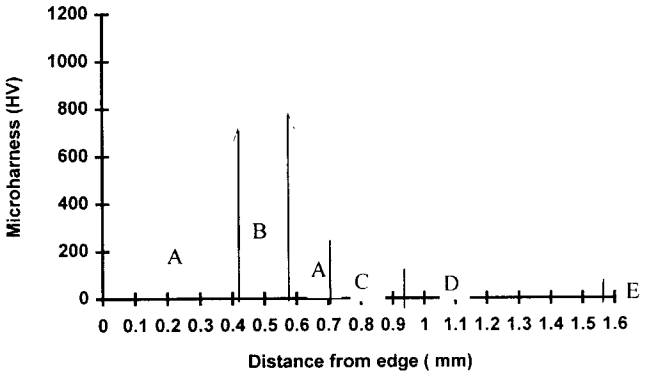

Fig. 8 Distribution of microhardness from the surface to the substrate

are a lot of phases in the alloyed zone: Al_3Ni_2, NiAl, Ni_3Al, and carbide $Cr_{23}C_6$. The major phase is WC, while FeAl and Fe_3Al are minor. This result is similar to that from microprobe analysis.

Figure 6(a) is a TEM photo in the laser-alloyed zone and Fig. 6(b) is its diffraction pattern. The main feature is an amorphous halo pattern whose area is much greater than the bright central area.

Figure 7(a) is a TEM photo of the fine granular region in the laser-melted zone. Figures 7(b) and (c) are its diffraction pattern and indexing, respectively. We can see two sets of crystalline pattern and amorphous halo. The indexing shows two types of crystalline Ni_3Al pattern, a face-centered cubic structure(Ni_3Al) and a tetragonal structure ($Ni_3Al(T)$). This implies that these three structures coexist in this region.

3.3 *Distribution of Hardness*

Figure 8 shows the distribution in microhardness from the surface of the laser-melted zone to the substrate. In this figure, part A is the needlelike structure region, part B is the fine granular structure region, part C is the transition layer, part D is the laser-melted Al-Si alloy region, and part E is the Al-Si alloy substrate. From this figure, the average microhardness of part A is 470 HV, which is 64% higher than that of the plasma-sprayed zone (286 HV). However, the microhardness of the fine granular region (part B) is high, up to 1027 HV, which is 3.6 times as much as that of the plasma-sprayed zone. Beneath the alloy zone, the microhardness of the laser-melted aluminum alloys (part D) is 128 HV, which is about 1.7 times as much as that of the original aluminum alloys (75 HV). The microhardness of the transition region (part C) is between that of part A and part D. This distribution of microhardness is of benefit to wear resistance.

4. Conclusion

A microscopic metallurgical examination was conducted on a Ni-WC surface layer that had been initially plasma sprayed on an Al-Si alloy and subsequently remelted with a CO_2 laser. The main finding is that a distinct layer exists about 0.5 mm beneath the top surface, the hardness of which is 1030 HV compared to 75 HV for the base Al-Si alloy. This layer may be useful in improving the wear-abrasion resistance of the Al-Si alloy.

Acknowledgment

The project was supported by the National Laboratory Foundation of Corrosion Science of the Institute of Corrosion and Protection of Metals, Academia Sinica, Shenyang, China.

References

1. M. Boas, M. Bamberger, and G. Revez, Laser-Alloying a Plasma-Sprayed WC/Co Layer to Enhance Wear Properties, *Surface and Coating Technology,* Vol 42, 1990, p 175-186
2. M.G. Pujar, R.K. Dayal, and R.K. Singh Raman, Microstructural and Aqueous Corrosion Aspects of Laser-Surface-Melted type 304ss Plasma-Coated Mild Steel, *Journal of Materials Engineering and Performance,* Vol 3, 1994, p 412-418
3. J. de Damborenea, V. Lopez, and A.J. Vazpuez, Improving High-Temperature Oxidation of Incoloy 800H by Laser Cladding, *Surface and Coating Technology,* Vol 70, 1995, p 107-113
4. D. Pantellis, E. Giannetaki, Y. Chryssoulakis, and P. Ponthiaux, Laser Surface Treatment of Aluminum Alloy 6061 with SiC Powder Injection, *Plating and Surface Finishing,* Vol 81, 1994, p 52-56
5. W.J. Tomlinson and A.S. Bransden, Cavitation Erosion of Laser Surface Alloyed Coatings on Al-12%Si, *Wear,* Vol 185, 1995, p 59-65
6. A. Almeida, M. Anjos, R. Vilar, R. Li, G.S. Ferreira, W.M. Steen, and K.G. Watkins, Laser Alloying of Aluminium Alloys with Chromium, *Surface and Coating Technology,* Vol 70, 1995, p 221-229
7. T.B. Massalski, *Binary Alloy Phase Diagrams,* American Society for Metals, 1986, p 142